Heliyon

Received:
29 October 2018
Revised:
28 February 2019
Accepted:
4 April 2019

Cite as: Swagatam Sarkar, Mitali Sarkar. Ultrasound assisted batch operation for the adsorption of hexavalent chromium onto engineered nanobiocomposite. Heliyon 5 (2019) e01491. doi: 10.1016/j.heliyon.2019.e01491

Ultrasound assisted batch operation for the adsorption of hexavalent chromium onto engineered nanobiocomposite

Swagatam Sarkar, Mitali Sarkar*

Department of Chemistry, University of Kalyani, Kalyani 741235, West Bengal, India

* Corresponding author.

E-mail address: msarkar@klyuniv.ac.in (M. Sarkar).

Abstract

The study demonstrates the comparative retention characteristics of chromium from aqueous environment on iron(III) cellulose nanocomposite bead under conventional (C-ads) and ultrasound assisted (U-ads) batch adsorption operation. Optimization of process parameters was achieved varying pH, contact/sonication time, initial Cr(VI) concentration, adsorbent dose at fixed solution temperature. Equilibrium was achieved within 5 h and 30 min of contact time in C-ads and U-ads respectively. Langmuir isotherm is found suitable in C-ads while Temkin in U-ads. Both the operation is aided by change in negative free energy, positive enthalpy and entropy. Ultrasound assisted adsorption is much favorable in terms of efficiency, feasibility, spontaneity and randomness. Both the operations follow more the second order than the first order kinetic model. The pore diffusion prevails more in case of U-ads while the surface adsorption in C-ads.

Keywords: Materials science, Chemistry, Analytical chemistry, Chemical engineering, Inorganic chemistry, Physical chemistry

https://doi.org/10.1016/j.heliyon.2019.e01491
2405-8440/© 2019 Published by Elsevier Ltd. This is an open access article under the CC BY-NC-ND license (http://creativecommons.org/licenses/by-nc-nd/4.0/).

1. Introduction

Advent of human civilization has resulted generation of large amount of wastewater containing a wide range of toxic chemicals including heavy metals, among which chromium is studied in the present report. Chromium, particularly in hexavalent oxidation state, may cause kidney damage, lung tumor, severe diarrhoea, allergic dermatitis, skin irritation, internal haemorrhage and respiratory problems (Mohan et al., 2005). A large amount of chromium is discharged from different industries viz. leather, mining, metallurgical (steel, ferrous- and nonferrous alloys), refractory (chrome and chrome-magnetite), electroplating, tannery, timber treatment and chemical (Dubey and Gopal, 2007). Treatment of chromium containing wastewater becomes a high priority issue to safeguard the environment and the lives on the earth (Nithya and Sudha, 2016).

Water pollution control technologies include coagulation, precipitation, sedimentation, filtration, solvent extraction, ion exchange, adsorption, electrodialysis and membrane separation (Mohan and Pittman Jr., 2006). However, adsorption is considered more acceptable in terms of convenience, ease of operation and simplicity in design (Babel and Kurniawan, 2003). Cellulose, the natural polysaccharide that is abundant in nature may be used as the precursor for synthesis of adsorbent with good capacity. The reactivity depends on the resultant cellulose structure where the monomeric cellulose units aggregate via the Van der Waals force as well as intra and intermolecular hydrogen bonding.

Cellulose based materials are used for adsorption of chromium by several researchers. Mechanical aid such as sonication applied to conventional process is supposed to improve the adsorption efficiency due to the increased solute mass transfer through acoustic waves (Roosta et al., 2014; Reddy et al., 2010). In the present report the behavior of iron modified cellulose nonocomposite (FeCNB) toward retention of chromium(VI) is compared in conventional (C-ads) and ultrasound assisted (U-ads) batch adsorption operation. The isotherm, thermodynamic feasibility and kinetics of operation were evaluated. The present authors find only four references of ultrasound assisted (sono) adsorption of chromium, yet the adsorbents are not cellulose based (Jing et al., 2011; Zhang et al., 2014; Zhou et al., 2016; Chen et al., 2017). Moreover, all these studies dealt with lower concentration of chromium, required higher time or stronger ultrasonic power, compared to the present report.

2. Experimental

2.1. Materials

All the chemicals and solvents used are of analytical grade (Merck, India). Cellulose powder (Loba Chemie, India) was used for the preparation of cellulose

https://doi.org/10.1016/j.heliyon.2019.e01491
2405-8440/© 2019 Published by Elsevier Ltd. This is an open access article under the CC BY-NC-ND license (http://creativecommons.org/licenses/by-nc-nd/4.0/).

nanocomposite bead. Chromium(VI) stock solution ($1.0.10^{-3}$ M) was prepared by dissolving appropriate amount of $K_2Cr_2O_7$ in deionized water and working solutions were prepared by proper dilution of the stock. Iron impregnation of cellulose bead was made with $Fe(NO_3)_3 \cdot 9H_2O$ solution (10 % W/V).

2.2. Preparation of FeCNB

Iron(III) loaded cellulose nanocomposite bead was synthesized in two steps; synthesis of cellulose nanocomposite bead (CNB) and modification of CNB with Fe(III).

CNB was synthesized by sol-gel transformation (Hench and West, 1990). Cellulose powder (1.0 g) was soaked in NaOH (20.0 cm^3, 19%) and was kept in an air free condition at room temperature for 8 h. On addition of CS_2 (1.0 cm^3) to the suspension and shaking (150 spm, 8 h) the cellulose xanthate (orange-yellow) was formed. Further addition of NaOH (10.0 cm^3, 6%) with continuous shaking for 6 h leads to the formation of a sol (red-brownish) that transformed into gel after keeping for 3 days. When the gel was added drop wise under stirring to a mixture of CH_3OH:-NaOH:H_2O::50:30:20 the cellulose nanocomposite bead (CNB) was appeared (Santra et al., 2014). CNB on repeated washing with de-ionized water turned snow white in color and kept under water at room temperature. In the next step CNB were modified with Fe(III). The solution of $Fe(NO_3)_3 \cdot 9H_2O$ (10%, w/v) was added under stirring (100 spm) at room temperature for 2 h to CNB and iron(III) loaded cellulose nanocomposite bead (FeCNB), red in color, was formed. The beads were washed repeatedly with de-ionized water and stored under water at room temperature. The color and shape of the beads remain stable at least for 90 days (Sarkar and Sarkar, 2017).

2.3. Characterization of FeCNB

The physicochemical, surface and thermal properties are evaluated for the characterization of the synthesized beads (Sarkar and Sarkar, 2017).

2.4. Batch operation protocol

Batch experiment was conducted to determine the influence of pH, FeCNB dose, agitation/sonication time and speed, initial Cr(VI) concentration at constant temperature on Cr(VI) uptake and retention. The range of operation was: pH (2−10), dose (0.5−5.0 g dm^{-3}), contact time (for C-ads; 0.5−5 h) and sonication time (for U-ads; 0.5−2.0 h), agitation speed (50−200 spm), initial Cr(VI) concentration (100−300 mg dm^{-3}), temperature of 290−310 K. Ultrasound assisted batch adsorption study was performed in a sonication bath (TRANS-O-SONIC; model: D-Compact, 30 cm × 20 cm × 30 cm, capacity: 1.5 dm^3, heater power 100 W). A definite amount of adsorbent (0.05 g) and Cr(VI) of known concentration (10 cm^3) was placed in a

https://doi.org/10.1016/j.heliyon.2019.e01491
2405-8440/© 2019 Published by Elsevier Ltd. This is an open access article under the CC BY-NC-ND license (http://creativecommons.org/licenses/by-nc-nd/4.0/).

temperature controlled water jacketed glass vial. An ultrasound wave of frequency 22.5 kHz, 120 W and total acoustic power of 1.52 W/cm^2 was applied for 10 min and the solution was shaken with controlled speed to attain the equilibrium.

The solution after equilibrium was filtered through Whatman 41 filter paper and the Cr(VI) concentration was determined in the filtrate spectrophotometrically (Perkin Elmer 7200A) via complexation with 1,5-diphenylcarbazide at 540 nm. The concentration of total chromium [Cr(VI) + Cr(III)], on the other hand, was determined by flame atomic absorption spectroscopy (FAAS; Perkin−Elmer 5100 PC) at 357.9 nm and a slit of 0.7 nm (APHA, 1995).

All the experiments were carried out in triplicate and the mean was taken. The efficiency of FeCNB is estimated by the extent of retention in percentage at equilibrium condition. Retention percent (RP) is calculated from the Eq. (1) and the equilibrium amount of Cr(VI) adsorbed, q_e (mg g^{-1}), is calculated from Eq. (2).

$$RP = \frac{(C_0 - C_e)}{C_0} \times 100 \quad (1)$$

$$q_e = \frac{(C_0 - C_e)}{m} \times V \quad (2)$$

where, C_0 and C_e are the initial and equilibrium Cr(VI) concentration (mg dm^{-3}) respectively, m is the mass of FeCNB (g) and V is the volume (dm^3) of solution.

3. Results and discussion

3.1. Characterisation of FeCNB

The physicochemical character of FeCNB was illustrated elsewhere (Sarkar and Sarkar, 2017). The porosity, degree of swelling and surface area values indicated the possible adsorption ability of FeCNB. In FeCNB presence of characteristics IR peaks of cellulose alongwith those corresponding to Fe-O stretching and O-Fe-O bending were observed. Scanning electron microscopy (SEM) study at different magnifications reveals spherical shape and nanonature of FeCNB with particle size of 60 nm. Electron dispersive X-ray spectrum (EDS) shows presence of C, O and Fe. The nanonature of the particles having mean diameter of 5 nm was indicated from Tranmission electron microscopy (TEM). The 2D topography of atomic force microscopy (AFM) image also supports nano surface structure with non regular distribution. Electron paramagnetic resonance (EPR) study indicates that isolated Fe(III) is present as free high spin state at the rhombic site. Thermogravimetric analysis-differential thermal analysis (TGA-DTA) study suggests stability of the bead at least upto 278 °C.

https://doi.org/10.1016/j.heliyon.2019.e01491
2405-8440/© 2019 Published by Elsevier Ltd. This is an open access article under the CC BY-NC-ND license (http://creativecommons.org/licenses/by-nc-nd/4.0/).

3.2. Influence of operational parameters in batch operation

3.2.1. Influence of pH

The pH dependent retention pattern of Cr(VI) in C-ads and U-ads is demonstrated in Fig. 1a. Adsorption is considered to be governed by the surface charge of FeCNB and the chromium species present in the solution. Considering the pH_{ZPC} of FeCNB (7.58) and speciation of chromium it is expected that in the pH range of 3−6 higher retention occurs due to the electrostatic attraction between FeCNB-$HCrO_4^-$. In higher pH lesser retention is due to repulsive interaction between the adsorbent and the anionic Cr(VI) species (Sarkar and Sarkar, 2017). It is interesting to note that retention of total chromium [Cr(VI) + Cr(III)] does not differ from that of

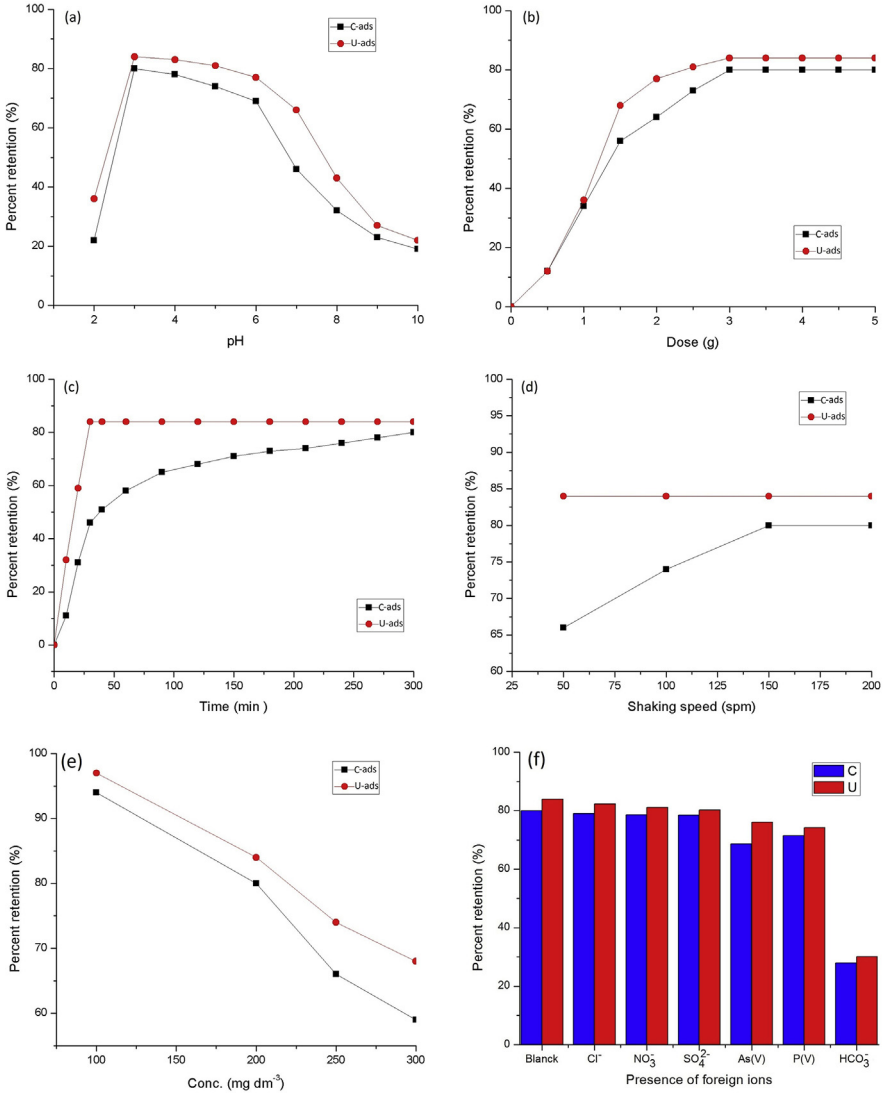

Fig. 1. Influence of operational parameters for C-ads and U-ads; (a) pH, (b) dose, (c) time, (d) shaking speed, (e) initial concentration, (f) coexisting anions.

https://doi.org/10.1016/j.heliyon.2019.e01491
2405-8440/© 2019 Published by Elsevier Ltd. This is an open access article under the CC BY-NC-ND license (http://creativecommons.org/licenses/by-nc-nd/4.0/).

Cr(VI) indicating that FeCNB is specific for Cr(VI) adsorption. Though the retention trend is found similar the extent at each pH is higher in case of U-ads compared to that in C-ads. However, the optimum pH is found to be 3.1 for both the operations.

3.2.2. Influence of adsorbent dose

Fig. 1b illustrates the retention profile of Cr(VI) with increasing FeCNB dose in U-ads compared to that in C-ads. With increasing dose the extent of Cr(VI) retention increases and reaches the maximum value at the optimum dose of 3.0 g dm^{-3} for both C-ads and U-ads. As the dose increases the number of active sites and also Cr(VI) retention on FeCNB surface increases. The saturation of retention even with increase of dose beyond equilibrium may be due to either aggregation or overlapping of active surface sites. Similar observation was reported by He et al. (2014), for adsorption of Cr(VI) on functionalized cellulose nanofiber.

3.2.3. Influence of contact time

In order to achieve Cr(VI)-FeCNB equilibrium the agitation period was varied and the retention behavior in U-ads was compared with that in C-ads. Initially the rate of retention is more which slows down gradually and reaches maximum near equilibrium (Fig. 1c). The increased retention is due to availability of more vacant adsorption sites and high solute concentration gradient between the adsorbent surface and bulk solution (Dehghani et al., 2015). The equilibrium is observed at 5 h and 30 min of contact time in C-ads and U-ads respectively. It is expected that ultrasonic irradiation enhances the solute mass transfer rate around the liquid-solid interfaces due to the high-pressure shock waves during the violent collapse of cavitation bubbles (Zhang et al., 2014). Thus, sonication develops equilibrium in shorter period than the conventional operation.

3.2.4. Influence of shaking speed

As reported earlier with increase in agitation speed from 50 to 200 spm Cr(VI) retention increases progressively from 38 to 80% in case of C-ads (Sarkar and Sarkar, 2017) due to enhanced diffusion rate of solute (Bankar et al., 2009). Interestingly, in case of U-ads the retention was found to be higher (84%), even with the lower agitation speed (50 spm) and does not alter with increase in agitation speed (Fig. 1d). Thus, ultrasound produces enough translational motion to the solution for Cr(VI) retention onto the FeCNB surface via acoustic streaming (Yang, 2001).

3.2.5. Influence of initial concentration

The present study was conducted at the optimum condition with different Cr(VI) concentrations (100−300 mg dm^{-3}) (Fig. 1e). The percent retention is higher for

https://doi.org/10.1016/j.heliyon.2019.e01491
2405-8440/© 2019 Published by Elsevier Ltd. This is an open access article under the CC BY-NC-ND license (http://creativecommons.org/licenses/by-nc-nd/4.0/).

lower initial concentration and vice versa in U-ads similar to C-ads. Similar observation was made by Gorzin and Rasht Abadi (2018) for Cr(VI) adsorption on paper mill sludge. However, higher percent retention was found in case of U-ads than C-ads, as sonication leads to more solute mass transfer via acoustic cavitations (Ansari et al., 2016).

3.2.6. Influence of coexisting anions

The role of common anions, present in the effluents such as nitrate, chloride and sulfate, on Cr(VI) retention using a fixed initial concentration (200 mg dm^{-3}) is studied for U-ads similar to the case of C-ads. It shows no significant influence of the studied anions load up to 10 times of Cr(VI). Fig. 1f compares the retention extent of Cr(VI) for C-ads and U-ads in presence of foreign anions. The lower retention in presence of AsO_4^{3-} and PO_4^{3-} is thought to be due to the competitive retention for adsorption sites (Neagu, 2009) while lower retention in presence of bicarbonate is due to increase of solution pH from 3.8 to 7.9.

3.2.7. Comparison of efficiency and operational parameters of different adsorbents

There are several reports for adsorptive removal of Cr(VI) from water. The efficiency depends on the operational condition. The performance of some cellulose based adsorbents in conventional operation is compared with the present adsorbent in Table 1.

3.3. Adsorption isotherm

Adsorption isotherm being useful for designing adsorption as a unit operation, different models Langmuir, Freundlich and Temkin are tested in the present case.

The Langmuir isotherm is used to estimate the monolayer adsorption capacity on homogeneous adsorbent sites (Langmuir, 1916) and is given as:

$$q_e = \frac{QbC_e}{1 + bC_e} \tag{3}$$

The linear form is presented as,

$$\frac{C_e}{q_e} = \frac{1}{Qb} + \frac{C_e}{Q} \tag{4}$$

where, Q (mg g^{-1}) and b (dm^3 mg^{-1}) are the maximum adsorption capacity and adsorption intensity respectively. C_e (mg dm^{-3}) and q_e (mg g^{-1}) represent residual Cr(VI) concentration and amount of Cr(VI) adsorbed on FeCNB at equilibrium respectively.

https://doi.org/10.1016/j.heliyon.2019.e01491
2405-8440/© 2019 Published by Elsevier Ltd. This is an open access article under the CC BY-NC-ND license (http://creativecommons.org/licenses/by-nc-nd/4.0/).

Table 1. Adsorption characteristics of reported adsorbents.

Sl no	Adsorbent	Operational parameters					Adsorption capacity	References
		pH	Time	Dose	Conc.	Temp		
1	Succinylated mercerized cellulose functionalized with quaternary ammonium groups	3.1	300 min.		1.92 mmol dm^{-3}	298 K	–	Gurgel et al. (2009)
2	Cellulose modified with β-CD and quaternary ammonium groups	4.5	10 min.	50 mg dm^{-3}	50 mg dm^{-3}	301 K	61.05 mg g^{-1}	Zhou et al. (2011)
3	Cellulose microsphere-based adsorbent prepared by radiation-induced grafting	3	15 min.	1 g dm^{-3}	100 mg dm^{-3}	298 K	78 mg g^{-1}	Li et al. (2012)
4	Cellulose modified with D-glucose quaternary ammonium groups	3.5	90 min.	50 mg dm^{-3}	50 mg dm^{-3}	291 K	71.79 mg g^{-1}	Zhou et al. (2012)
5	Cellulose grafted with acrylonitrile monomer	5	300 min.	6 g dm^{-3}	200 mg dm^{-3}	298 K	371.96 mg g^{-1} 86 %	Hajeeth et al. (2014)
6	Quaternary ammonium functionalized cellulose nanofiber aerogels	3	50 min.	1 g dm^{-3}	1 mg dm^{-3}	298 K	17.66 mg g^{-1}	He et al. (2014)
7	Polyaniline/bacterial extracellular polysaccharide nanocomposite	3	50 min.	0.1 g dm^{-3}	25 mg dm^{-3}	298 K	304.5 mg g^{-1}	Janaki et al. (2014)
8	Glycidyl methacrylate grafted onto cellulose	3	180 min.	1 g dm^{-3}	30 mg dm^{-3}	333 K	500 mg g^{-1}	Lin et al. (2014)
9	Cellulose derived magnetic mesoporous carbon nanocomposites	1	10 min.	2.5 g dm^{-3}	4 & 1000 mg dm^{-3}	298 K	293.8, 327.5 mg g^{-1}; 98.1, 93.5 %	Qiu et al. (2014)
10	Graft copolymer of cellulose extracted from sisal fibre with acrylic acid monomer	5	360 min.	4 g dm^{-3}	200 mg dm^{-3}	303 K	4.53, 5.28 mg g^{-1}	Hajeeth et al. (2015)
11	Chitosan/carboxyl methyl cellulose/silica hybrid membrane	1.3	60 min.	0.3 g dm^{-3}	120 mg dm^{-3}	333 K	16.08 mg g^{-1}	He et al. (2015)
12	Chemically modified natural cellulose	1	120 min.	–	400 mg dm^{-3}	343 K	32.4 mg g^{-1}	Zhu et al. (2015)
13	Treated waste news paper	3	60 min.	3 g dm^{-3}	20 mg dm^{-3}	318 K	59.88 mg g^{-1}	Dehghani et al. (2016)
14	Polyethylenimine-functionalized cellulose aerogel beads	2	180 min.	0.02 g dm^{-3}	100 mg dm^{-3}	298 K	229.1 mg g^{-1}	Guo et al. (2017)
15	Nanosized cellulose fibers from rice husk	6	100 min.	1.5 g dm^{-3}	30 mg dm^{-3}	303 K	3.76 mg g^{-1}	Pourfadakari et al. (2017)
16	Starch and sodium carboxymethyl cellulose-coated Fe and Fe/Ni nanoparticles	2	120 min.	1 g dm^{-3}	1 mg dm^{-3}	298 K	95.70%	Wang et al. (2018)
17	Iron(III) cellulose nanocomposite bead for C-ads & U-ads	3.1	300, 30 min.	3 g dm^{-3}	200 mg dm^{-3}	300 K	141, 211 mg g^{-1}	Present study

https://doi.org/10.1016/j.heliyon.2019.e01491

2405-8440/© 2019 Published by Elsevier Ltd. This is an open access article under the CC BY-NC-ND license (http://creativecommons.org/licenses/by-nc-nd/4.0/).

Freundlich adsorption is employed to estimate the adsorption intensity of the adsorbent towards heterogeneous adsorbent sites (Freundlich, 1906). It can be expressed as:

$$q_e = K_F C_e^{\frac{1}{n}} \tag{5}$$

The linear form is presented as,

$$\ln q_e = \ln K_F + \frac{1}{n} \ln C_e \tag{6}$$

where, K_F ((g mg^{-1}) (mg $dm^{-3})^{-1/n}$) is the Freundlich constant related to the adsorption capacity and 1/n is adsorption intensity, indicating the affinity or binding strength.

Temkin isotherm assumes that decay of the heat of solute adsorption on the adsorbent layer with surface coverage, due to solute−adsorbent interaction, is linear rather than logarithmic, in contrast to the Freundlich equation (Temkin and Pyzhev, 1940). It can be expressed as follows:

$$q_e = \left(\frac{RT}{B_T}\right) \ln A_T \cdot C_e \tag{7}$$

On linearization it takes the form as,

$$q_e = \left(\frac{RT}{B_T}\right) \ln A_T + \left(\frac{RT}{B_T}\right) \ln C_e \tag{8}$$

where, A_T is the equilibrium binding constant corresponding to the maximum binding energy (dm^3 mg^{-1}), B_T is related to the heat of sorption (J mol^{-1}), R is the molar gas constant (8.314×10^{-3} kJ mol^{-1} K^{-1}), T is the absolute temperature (K).

The isotherm study was performed under equilibrium condition and the constants for U-ads and C-ads are compared in Table 2. The adsorption capacity corresponding to each isotherm (Q, K_F, A_T) is found higher in case of U-ads than in case of C-ads, indicating better performance of ultrasound assisted operation. The equilibrium parameter q_e corresponding to each isotherm was compared with the experimental q_e and compared in Fig. 2a for C-ads and in Fig. 2b for U-ads.

3.4. Isotherm validity testing using statistical parameters

It is found that in case of U-ads R^2 values for Langmuir and Temkin are comparable and higher than Freundlich model in contrast to the case of C-ads, where the R^2 value for Langmuir is reported to be highest compared to Freundlich and Temkin. The validity of a particular isotherm model for the present solute−adsorbent interaction is primarily judged from the correlation coefficient value (R^2) using linear regression.

https://doi.org/10.1016/j.heliyon.2019.e01491
2405-8440/© 2019 Published by Elsevier Ltd. This is an open access article under the CC BY-NC-ND license (http://creativecommons.org/licenses/by-nc-nd/4.0/).

Table 2. Isotherm constants for C-ads and U-ads.

Isotherm	T (K)	Q.10^{-2} (mg g^{-1})		b (dm^3 mg^{-1})		R^2		χ^2	
		C-ads	U-ads	C-ads	U-ads	C-ads	U-ads	C-ads	U-ads
Langmuir	290	1.265	2.002	1.165	09.96	0.9969	0.9831	0.0044	0.0046
	300	1.410	2.110	2.894	16.52	0.9971	0.9840	0.0059	0.0184
	310	1.522	2.281	7.141	24.22	0.9990	0.9821	0.0118	0.0268
	T (K)	K_F (g mg^{-1}) (mg dm^3)$^{-1/n}$		1/n		R^2		χ^2	
		C-ads	U-ads	C-ads	U-ads	C-ads	U-ads	C-ads	U-ads
Freundlich	290	65.64	98.80	0.2761	0.185	0.9052	0.9692	0.0436	0.0247
	300	68.87	77.41	0.2880	0.213	0.8946	0.9740	0.0529	0.0642
	310	74.38	61.38	0.2703	0.238	0.8192	0.9531	0.0757	0.0454
	T (K)	A_T (dm^3 mg^{-1})		B_T (J mol^{-1})		R^2		χ^2	
		C-ads	U-ads	C-ads	U-ads	C-ads	U-ads	C-ads	U-ads
Temkin	290	15.11	34.66	13.69	8.831	0.8960	0.9898	0.0071	0.0011
	300	15.22	83.31	12.35	8.314	0.9141	0.9854	0.0152	0.0103
	310	25.60	103.3	12.51	8.130	0.9123	0.9849	0.0210	0.0016

4 significant digits.

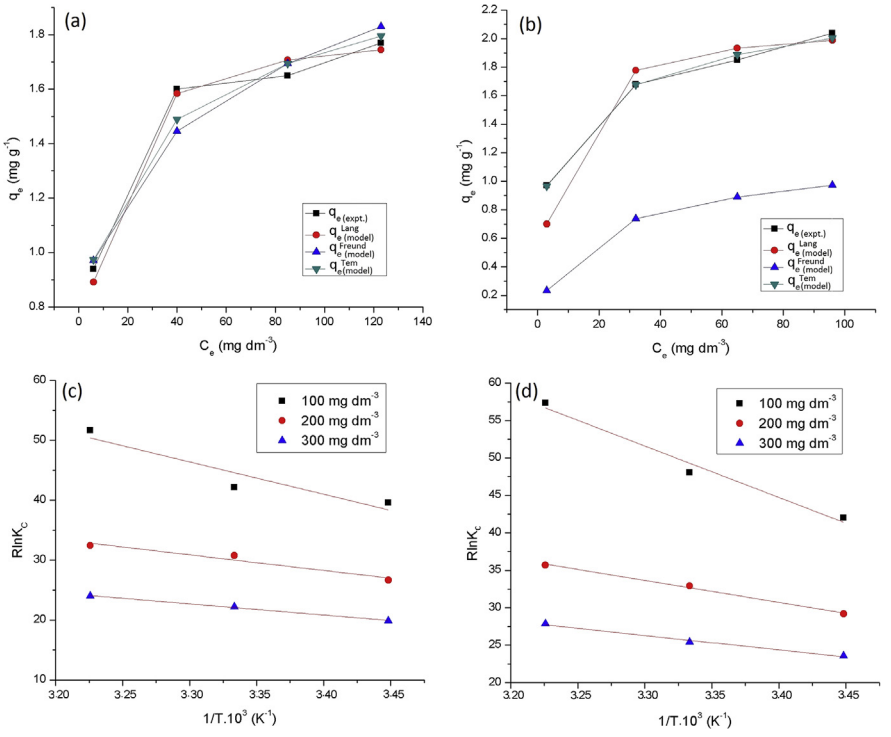

Fig. 2. Plot of C_e against q_e for (a) C-ads, (b) U-ads; Plot of van't Hoff equation for (c) C-ads, (d) U-ads.

https://doi.org/10.1016/j.heliyon.2019.e01491
2405-8440/© 2019 Published by Elsevier Ltd. This is an open access article under the CC BY-NC-ND license (http://creativecommons.org/licenses/by-nc-nd/4.0/).

Linear regression considers that the standard deviations (differences between the measured and the calculated values) are equal in each point. But, during linearization of nonlinear form, the unity standard deviation in points of the linear form deviates. This implies that the theories behind the model giving the best fitting parameters for the linear form not necessarily for the original nonlinear one. Therefore, nonlinear regression is the most feasible method to estimate isotherm model parameters (Ho, 2004a). In the present case, Chi square analysis is performed to find the best fitted isotherm model. The advantage of using Chi square test is the possibility of comparison of all isotherms on the same abscissa and ordinate.

The Chi-square (χ^2) value is calculated (Naiya et al., 2009) using Eq. (8) as,

$$\chi^2 = \sum_{i=1}^{n} \frac{\left(q_{e,calc} - q_{e,meas}\right)^2}{q_{e,meas}} \tag{9}$$

Based on such analysis (Table 2) it reveals that in case of C-ads the trend of data fit follows: Langmuir > Temkin > Freundlich. It suggests that Cr(VI) adsorption takes place at specific homogeneous sites of FeCNB. Moreover, higher Q and b values at higher temperatures indicate more capacity and affinity of Cr(VI) on FeCNB due to surface activation. Similar report was made by Anandkumar and Mandal (2011). Interestingly, in case of U-ads, Temkin isotherm is most acceptable and the trend is Temkin > Langmuir >> Freundlich. The Temkin isotherm contains a factor that explicitly takes into the account solute-adsorbent interactions. The ultrasonication, due to cavitation effect, leads to uniform distribution of binding energies (Milenković et al., 2013) and the heat of solute adsorption is expected to decrease linearly with surface coverage during solute-adsorbent interaction.

3.5. Feasibility of adsorption

The feasibility of Cr(VI)-FeCNB interaction may be evaluated from the separation factor (SF), a dimensionless quantity (Ozdemir et al., 2004), which is expressed as,

$$SF = \frac{1}{1 + b.C_0} \tag{10}$$

where, b is the Langmuir isotherm constant and C_0 is the initial Cr(VI) concentration in solution. The SF value may reveal the nature of the isotherm (Lin et al., 2014), as favorable ($0 < SF < 1$), irreversible ($SF = 0$), unfavorable ($SF > 1$) or linear ($SF = 1$).

In the present case of U-ads the SF values at different temperatures and concentrations are found to lie between 0 and 1, similar to the case of C-ads, indicating favorable case of adsorption for both the cases. Thermodynamic feasibility was tested from the change of Gibbs free energy (ΔG); Eq. (11). The change in enthalpy

https://doi.org/10.1016/j.heliyon.2019.e01491
2405-8440/© 2019 Published by Elsevier Ltd. This is an open access article under the CC BY-NC-ND license (http://creativecommons.org/licenses/by-nc-nd/4.0/).

(ΔH) and entropy (ΔS) was evaluated from the slope and intercept respectively of the plot of the van't Hoff Eq. (12) (Ali et al., 2016),

$$-\Delta G = RTlnK_C \tag{11}$$

$$RlnK_C = -\frac{\Delta H}{T} + \Delta S \tag{12}$$

where, K_c is the equilibrium constant. It is found that the ΔG values are negative corresponding to all studied Cr(VI) concentrations (Table 3). Thus both the operations are said to be spontaneous. Moreover, higher magnitude of −ΔG in case of U-ads compared to C-ads indicates more feasibility of the former operation. Increase in the values of −ΔG with an increase in temperature suggests more Cr(VI) adsorption at higher temperatures. Plot of van't Hoff equation for C-ads is presented in Fig. 2c and that of U-ads in Fig. 2d. Both the ΔH and ΔS are found to be positive for each concentration of chromium and in each operation (Table 3). Thus, the operations are endothermic and random in nature. The endothermic nature is also indicated by the increased extent of adsorption with temperature rise. The increased randomness (more ΔS) indicates that the U-ads is preferred than the C-ads.

3.6. Adsorption kinetics

The nature of the adsorption process may depend on physical and chemical characteristics of the adsorbent as well as the system conditions. The pseudo first- and second-order models were tested to find the rate and mechanism of solute−adsorbent interaction.

3.6.1. Pseudo first order (Lagergren) rate equation

The integrated pseudo-first order rate equation, also known as Lagergren rate equation (Ho, 2004b) is expressed as:

Table 3. Thermodynamic constants for C-ads and U-ads.

Conc. (mg dm^{-3})	Temp. (K)	−ΔG (kJ mol^{-1})		ΔH (kJ mol^{-1})		ΔS (kJ mol^{-1} K^{-1})	
		C-ads	U-ads	C-ads	U-ads	C-ads	U-ads
100	290	11.47	42.01	53.97	68.70	0.2241	0.2780
	300	12.94	48.04				
	310	16.01	57.34				
200	290	9.620	29.18	22.13	29.34	0.1092	0.1302
	300	10.83	32.93				
	310	11.81	35.70				
300	290	5.770	23.56	18.59	19.16	0.0844	0.0893
	300	6.670	25.41				
	310	7.440	27.83				

4 significant digits.

https://doi.org/10.1016/j.heliyon.2019.e01491
2405-8440/© 2019 Published by Elsevier Ltd. This is an open access article under the CC BY-NC-ND license (http://creativecommons.org/licenses/by-nc-nd/4.0/).

$$\ln(q_e - q_t) = \ln q_e - K_1 t \quad (13)$$

where, q_e and q_t are the amount of solute on adsorbent (mg g^{-1}) at equilibrium and time t respectively. K_1 represents the first order rate constant.

A plot of $\ln(q_e\text{-}q_t)$ against time (t) at a fixed temperature and initial solution concentration yields a straight line and K_1 can be evaluated from the slope. In Fig. 3a Lagergren plot of U-ads is compared with that of C-ads. The kinetic experiment was carried out at three different Cr(VI) concentrations (100, 200 and 250 mg dm^{-3}) for C-ads and U-ads. The value of K_1 is found to decrease with increased concentration (Table 4).

3.6.2. Pseudo second order rate equation

The linear form of the second order kinetic equation (Ho and McKay, 1999) is represented as,

$$\frac{t}{q_t} = \frac{1}{K_2 q_e^2} + \frac{t}{q_e} \quad (14)$$

where, K_2 is the second order rate constant (g mg^{-1} min^{-1}) and is evaluated from the intercept of the straight line plot of t/q_t against time (t) at fixed temperature and initial solute concentration. The values of K_2 corresponding to different initial

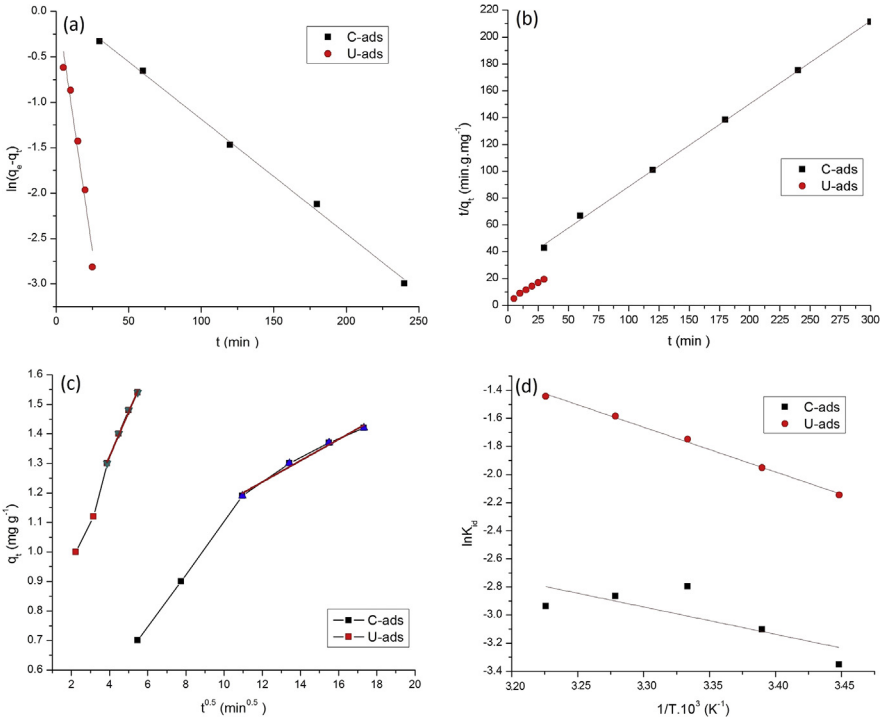

Fig. 3. Plot of (a) Pseudo first order rate equation, (b) Pseudo second order rate equation, (c) Intraparticle diffusion model (Weber-Morris) (d) Arrhenius equation.

https://doi.org/10.1016/j.heliyon.2019.e01491
2405-8440/© 2019 Published by Elsevier Ltd. This is an open access article under the CC BY-NC-ND license (http://creativecommons.org/licenses/by-nc-nd/4.0/).

Table 4. Rate parameters for C-ads and U-ads.

Equation	Conc. (mg dm^{-3})	$K_1.10^2$ (min^{-1})		R^2		χ^2	
		C-Ads	U-Ads	C-Ads	U-Ads	C-Ads	U-Ads
Pseudo 1st order	100	1.402	14.52	0.9911	0.9576	0.1313	0.2803
	200	0.8021	10.94	0.9970	0.9633	0.2511	0.1863
	250	1.011	7.513	0.8923	0.9733	0.1105	0.1130
	Conc. (mg dm^{-3})	**$K_2.10^2$ (g mg^{-1} min^{-1})**		**R^2**		**χ^2**	
		C-Ads	**U-Ads**	**C-Ads**	**U-Ads**	**C-Ads**	**U-Ads**
Pseudo 2nd order	100	2.721	16.45	0.9993	0.9924	0.0422	0.0793
	200	2.430	11.42	0.9971	0.9945	0.0003	0.0646
	250	1.811	8.201	0.9982	0.9814	0.0392	0.0717
	Conc. (mg dm^{-3})	**$K_{id}.10^2$ (g mg^{-1} min$^{-1/2}$)**		**Intercept 10^2**		**E_a (kJ mol^{-1})**		**R^2**	
		C-Ads	**U-Ads**	**C-Ads**	**U-Ads**	**C-Ads**	**U-Ads**	**C-Ads**	**U-Ads**
Weber Morris	100	3.521	11.72	34.73	32.44	15.78	2.532	0.9560	0.9611
	200	6.112	17.43	42.62	60.22			0.9560	0.9891
	250	5.302	20.50	63.80	56.13			0.9562	0.9883

4 significant digits.

concentrations are presented in Table 4. It is found that as the concentration increases the K_2 decreases. Fig. 3b represents similar nature but different profile for second order kinetic plots in U-ads and C-ads.

It is found that R^2 values for first and second order equations are comparable. Therefore, χ^2 values are evaluated to find the best data fit. The lower χ^2 values reveal that in both the operations adsorption interaction follows more the second order than the first order kinetic model. However, the rate parameter values are higher in case of U-ads than the C-ads.

3.6.3. Weber and Morris rate equation

The adsorption process is believed to follow a complex pathway and is accompanied by both surface and the pore diffusion, but in different extents. In order to examine the diffusion mechanism, the intraparticle diffusion model was analysed following the Weber and Morris equation (Cheung et al., 2007).

$$q_t = K_{id} t^{\frac{1}{2}} + C \tag{15}$$

where, K_{id} is the rate constant (mg g^{-1} min$^{-1/2}$) for pore diffusion (also called intraparticle diffusion coefficient) that indicates the extent of pore diffusion.

A plot of q_t against square root of time results an initial curved portion followed by a linear one near to equilibrium (Fig. 3c). The extrapolated linear portion of the curve

https://doi.org/10.1016/j.heliyon.2019.e01491
2405-8440/© 2019 Published by Elsevier Ltd. This is an open access article under the CC BY-NC-ND license (http://creativecommons.org/licenses/by-nc-nd/4.0/).

is characterized by a slope (K_{id}) and an intercept (C). The intercept reflects the extent of boundary layer effect. The larger the intercept the greater is the contribution of surface adsorption or boundary layer diffusion towards overall process. Magnitude of the intercept may be correlated with contribution of surface sorption in the rate controlling step (Abbas and Trari, 2015). The higher value of intraparticle diffusion coefficient (K_{id}) values in case of U-ads compared to C-ads (Table 4) is obtained. This indicates pore diffusion is more favorable in case of U-ads.

In an aim to provide an idea concerning feasibility of pore diffusion Arrhenius equation was employed as,

$$\ln K_{id} = \ln A - \frac{E_a}{RT} \tag{16}$$

where, E_a (kJ mol^{-1}) is the activation energy of the pore diffusion, A is Arrhenius frequency factor and T is the absolute temperature. The linear plot of $\ln K_{id}$ against 1/T (Fig. 3d) yields E_a from the slope, which is found to be 15.78 and 2.531 kJ mol^{-1} for C-ads and U-ads respectively. The lower value of E_a suggests that U-ads assisted more by pore diffusion. Acceleration in mass transfer phenomena by ultrasound application although is reported the mechanism is not fully understood. The liquid jets toward particle surfaces probably reduce the mass transfer limitations around solid particles that cause higher adsorption due to pushing of solute molecules into micropores, reaching to more active sites (Milenković et al., 2013).

4. Conclusion

Fe(III) loaded cellulose nanocomposite bead was found effective for retention of hexavalent chromium from aqueous solution. The performance of conventional batch operation was compared with ultrasound assisted adsorption experiment and the optimum condition for the process parameters such as pH, contact/sonication time, initial Cr(VI) concentration, dose at fixed solution temperature was evaluated. The equilibrium is achieved at pH 3, dose 3 g dm^{-3}, speed 150 spm within 300 minutes of contact time, in C-ads while at pH 3.5, dose 3 g dm^{-3}, speed 50 spm and 30 minutes in U-ads. Quick attainment of equilibrium and enhanced extent of retention in U-ads is due to enhanced mass transfer via translation motion, due to acoustic cavitation effect. It is found that in conventional adsorption Langmuir isotherm is most suitable whereas in ultrasound assisted adsorption Temkin isotherm is followed. Both the operation is aided by change in negative free energy, positive enthalpy and entropy. Ultrasound assisted adsorption is much more favorable in terms of efficiency, feasibility, spontaneity and randomness. Both the operations follow more the second order than the first order kinetic model. The energy parameter suggests that U-ads is assisted by pore diffusion while C-ads by surface adsorption.

https://doi.org/10.1016/j.heliyon.2019.e01491
2405-8440/© 2019 Published by Elsevier Ltd. This is an open access article under the CC BY-NC-ND license (http://creativecommons.org/licenses/by-nc-nd/4.0/).

Declarations

Author contribution statement

Mitali Sarkar: Conceived and designed the experiments; Analyzed and interpreted the data; Contributed reagents, materials, analysis tools or data; Wrote the paper.

Swagatam Sarkar: Performed the experiments; Analyzed and interpreted the data; Contributed reagents, materials, analysis tools or data; Wrote the paper.

Funding statement

This work was supported by the University of Kalyani.

Competing interest statement

The authors declare no conflict of interest.

Additional information

No additional information is available for this paper.

Acknowledgements

The authors sincerely acknowledge the assistance received under UGC-SAP, DST-FIST, DST-PURSE programs. Thanks are due to IACS, Kolkata for providing instrumental analysis.

References

Abbas, M., Trari, M., 2015. Kinetic, equilibrium and thermodynamic study on the removal of congo red from aqueous solutions by adsorption onto apricot stone. Process Saf. Environ. Protect. 98 (38), 424−436.

Ali, A., Saeed, K., Mabood, F., 2016. Removal of chromium (VI) from aqueous medium using chemically modified banana peels as efficient low-cost adsorbent. Alexandria Eng. J. 55 (3), 2933−2942.

Anandkumar, J., Mandal, B., 2011. Adsorption of chromium(VI) and Rhodamine B by surface modified tannery waste: kinetic, mechanistic and thermodynamic studies. J. Hazard. Mater. 186 (2-3), 1088−1096.

Ansari, F., Ghaedi, M., Taghdiri, M., Asfaram, A., 2016. Application of ZnO nanorods loaded on activated carbon for ultrasonic assisted dyes removal: experimental design and derivative spectrophotometry method. Ultrason. Sonochem. 33, 197−209.

https://doi.org/10.1016/j.heliyon.2019.e01491
2405-8440/© 2019 Published by Elsevier Ltd. This is an open access article under the CC BY-NC-ND license (http://creativecommons.org/licenses/by-nc-nd/4.0/).

APHA, AWWA, WEF, 1995. Standard Methods for the Examination of Water and Wastewater, nineteenth ed. United Book Press, Inc., Baltimore.

Babel, S., Kurniawan, T.A., 2003. Low-cost adsorbents for heavy metals uptake from contaminated water: a review. J. Hazard. Mater. B97 (1-3), 219–243.

Bankar, A.V., Kumar, A.R., Zinjarde, S.S., 2009. Removal of chromium (VI) ions from aqueous solution by adsorption onto two marine isolates of Yarrowia lipolytica. J. Hazard. Mater. 170 (1), 487–494.

Chen, L., Chen, Z., Chen, D., Xiong, W., 2017. Removal of hexavalent chromium from contaminated waters by ultrasound-assisted aqueous solution ball milling. J. Environ. Sci. 52, 276–283.

Cheung, W.H., Szeto, Y.S., McKay, G., 2007. Intraparticle diffusion processes during acid dye adsorption onto chitosan. Bioresour. Technol. 98 (15), 2897–2904.

Dehghani, M.H., Taher, M.M., Bajpai, A.K., Heibati, B., Tyagi, I., Asif, M., Agarwal, S., Gupta, V.K., 2015. Removal of noxious Cr(VI) ions using single-walled carbon nanotubes and multi-walled carbon nanotubes. Chem. Eng. J. 279 (48), 344–352.

Dehghani, M.H., Sanaei, D., Ali, I., Bhatnagar, A., 2016. Removal of chromium(VI) from aqueous solution using treated waste newspaper as a low-cost adsorbent: kinetic modeling and isotherm studies. J. Mol. Liq. 215, 671–679.

Dubey, S.P., Gopal, K., 2007. Adsorption of chromium(VI) on low cost adsorbents derived from agricultural waste material: a comparative study. J. Hazard. Mater. 145 (3), 465–470.

Freundlich, H.M.F., 1906. Over the adsorption in solution. J. Phys. Chem. 57, 385–471.

Gorzin, F., Abadi, M.M.B.R., 2018. Adsorption of Cr(VI) from aqueous solution by adsorbent prepared from paper mill sludge: kinetics and thermodynamics studies. Adsorpt. Sci. Technol. 36 (1-2), 149–169.

Guo, D.M., An, Q.D., Xiao, Z.Y., Zhai, S.R., Shi, Z., 2017. Polyethylenimine-functionalized cellulose aerogel beads for efficient dynamic removal of chromium(vi) from aqueous solution. RSC Adv. 7 (85), 54039–54052.

Gurgel, L.V.A., Perin de Melo, J.C., de Lena, J.C., Gil, L.F., 2009. Adsorption of chromium (VI) ion from aqueous solution by succinylated mercerized cellulose functionalized with quaternary ammonium groups. Bioresour. Technol. 100 (13), 3214–3220.

https://doi.org/10.1016/j.heliyon.2019.e01491
2405-8440/© 2019 Published by Elsevier Ltd. This is an open access article under the CC BY-NC-ND license (http://creativecommons.org/licenses/by-nc-nd/4.0/).

Hajeeth, T., Sudha, P.N., Vijayalakshmi, K., Gomathi, T., 2014. Sorption studies on Cr (VI) removal from aqueous solution using cellulose grafted with acrylonitrile monomer. Int. J. Biol. Macromol. 66, 295–301.

Hajeeth, T., Sudha, P.N., Vijayalakshmi, K., 2015. Removal of Cr (VI) from aqueous solution using graft copolymer of cellulose extracted from sisal fibre with acrylic acid monomer. Cellul. Chem. Technol. 49 (9-10), 891–900.

He, X., Cheng, L., Wang, Y., Zhao, J., Zhang, W., Lu, C., 2014. Aerogels from quaternary ammonium-functionalized cellulose nanofibers for rapid removal of Cr(VI) from water. Carbohydr. Polym. 111 (18), 683–687.

He, X.M., Xu, H.D., Li, H., 2015. Cr(VI) removal from aqueous solution by chitosan/carboxylmethyl cellulose/silica hybrid membrane. World J. Eng. Technol. 3 (3C), 234–240.

Hench, L.L., West, J.K., 1990. The sol-gel process. Chem. Rev. 90 (1), 33–72.

Ho, Y.S., 2004a. Selection of optimum sorption isotherm. Carbon 42 (10), 2115–2116.

Ho, Y.S., 2004b. Citation review of Lagergren kinetic rate equation on adsorption reactions. Scientometrics 59 (1), 171–177.

Ho, Y.S., McKay, G., 1999. Pseudo-second-order model for sorption processes. Process Biochem. 34 (5), 451–465.

Janaki, V., Shin, M., Kim, S., Lee, K., Cho, M., Ramasamy, A.K., Oh, B., Kamala-Kannan, S., 2014. Application of polyaniline/bacterial extracellular polysaccharide nanocomposite for removal and detoxification of Cr(VI). Cellulose 21 (1), 463–472.

Jing, G., Zhou, Z., Song, L., Dong, M., 2011. Ultrasound enhanced adsorption and desorption of chromium (VI) on activated carbon and polymeric resin. Desalination 279, 423–427.

Langmuir, I., 1916. The constitution and fundamental properties of solids and liquids. J. Am. Chem. Soc. 38 (11), 2221–2295.

Li, C., Zhang, Y., Peng, J., Wu, H., Li, J., Zhai, M., 2012. Adsorption of Cr(VI) using cellulose microsphere-based adsorbent prepared by radiation-induced grafting. Radiat. Phys. Chem. 81 (8), 967–970.

Lin, C., Qiao, S., Luo, W., Liu, Y., Liu, D., Li, X., Liu, M., 2014. Thermodynamics, kinetics and regeneration studies for adsorption of Cr(VI) from aqueous solutions using modified cellulose as adsorbent. BioResources 9 (4), 6998–7017.

https://doi.org/10.1016/j.heliyon.2019.e01491
2405-8440/© 2019 Published by Elsevier Ltd. This is an open access article under the CC BY-NC-ND license (http://creativecommons.org/licenses/by-nc-nd/4.0/).

Milenković, D.D., Bojić, A.L., Veljković, V.B., 2013. Ultrasound-assisted adsorption of 4-dodecylbenzene sulfonate from aqueous solutions by corn cob activated carbon. Ultrason. Sonochem. 20 (3), 955−962.

Mohan, D., Singh, K.P., Singh, V.K., 2005. Removal of hexavalent chromium from aqueous solution using low-cost activated carbons derived from agricultural waste materials and activated carbon fabric cloth. Ind. Eng. Chem. Res. 44 (4), 1027−1042.

Mohan, D., Pittman Jr., C.U., 2006. Activated carbons and low cost adsorbents for remediation of tri- and hexavalent chromium from water. J. Hazard. Mater. B137 (2), 762−811.

Naiya, T.K., Bhattacharya, A.K., Das, S.K., 2009. Clarified sludge (basic oxygen furnace sludge)-an adsorbent for removal of Pb(II) from aqueous solutions − kinetics, thermodynamics and desorption studies. J. Hazard. Mater. 170 (1), 252−262.

Nithya, R., Sudha, P.N., 2016. Removal of heavy metals from tannery effluent using chitosan-g-poly(butyl acrylate)/bentonite nanocomposite as an adsorbent. Text. Cloth. Sustain. 2 (7), 1−8.

Neagu, V., 2009. Removal of Cr(VI) onto functionalized pyridine copolymer with amide groups. J. Hazard. Mater. 171, 410−416.

Ozdemir, O., Armagan, B., Turan, M., Celik, M.S., 2004. Comparison of the adsorption characteristics of azo-reactive dyes on mezoporous minerals. Dyes Pigments 62 (1), 49−60.

Pourfadakari, S., Jorfi, S., Ahmadi, M., Takdastan, A., 2017. Experimental data on adsorption of Cr(VI) from aqueous solution using nanosized cellulose fibers obtained from rice husk. Data Brief 15, 887−895.

Qiu, B., Gu, H., Yan, X., Guo, J., Wang, Y., Sun, D., Wang, Q., Khan, M., Zhang, X., Weeks, B.L., Young, D.P., 2014. Cellulose derived magnetic mesoporous carbon nanocomposites with enhanced hexavalent chromium removal. J. Mater. Chem. A 2 (41), 17454−17462.

Reddy, B.R., Sivasankar, T., Sivakumar, M., Moholkar, V.S., 2010. Physical facets of ultrasonic cavitational synthesis of zinc ferrite particles. Ultrason. Sonochem. 17 (2), 416−426.

Roosta, M., Ghaedi, M., Daneshfar, A., Sahraei, R., Asghari, A., 2014. Optimization of the ultrasonic assisted removal of methylene blue by gold nanoparticles loaded on activated carbon using experimental design methodology. Ultrason. Sonochem. 21 (1), 242−252.

 https://doi.org/10.1016/j.heliyon.2019.e01491
2405-8440/© 2019 Published by Elsevier Ltd. This is an open access article under the CC BY-NC-ND license (http://creativecommons.org/licenses/by-nc-nd/4.0/).

Santra, D., Joarder, R., Sarkar, M., 2014. Taguchi design and equilibrium modeling for fluoride adsorption on cerium loaded cellulose nanocomposite bead. Carbohydr. Polym. 111 (10), 813−821.

Sarkar, M., Sarkar, S., 2017. Adsorption of Cr(VI) on Iron(III) cellulose nanocomposite bead. Environ. Process. 4 (4), 851−871.

Temkin, M.I., Pyzhev, V., 1940. Kinetics of ammonia synthesis on promoted iron catalysts. Acta Physiochim. URSS 12 (1), 217−222.

Wang, J., Ji, B., Shu, Y., Chen, W., Zhu, L., Chen, F., 2018. Cr(VI) removal from aqueous solution using starch and sodium carboxymethyl cellulose-coated Fe and Fe/Ni nanoparticles. Pol. J. Environ. Stud. 27 (6), 2785−2792.

Yang, R.T., 2001. Ultrasound enhanced adsorption and desorption of phenol on activated carbon and polymeric resin. Ind. Eng. Chem. Res. 40 (22), 4912−4918.

Zhang, W., Deng, M., Sun, C., Wang, S., 2014. Ultrasound-enhanced adsorption of chromium(VI) on Fe_3O_4 magnetic particles. Ind. Eng. Chem. Res. 53 (1), 333−339.

Zhou, Y., Jin, Q., Zhu, T., Akama, Y., 2011. Adsorption of chromium (VI) from aqueous solutions by cellulose modified with β-CD and quaternary ammonium groups. J. Hazard. Mater. 187 (1-3), 303−310.

Zhou, Y., Jin, Q., Zhu, T., Zhang, Q., Ma, T., 2012. Separation of chromium (VI) from aqueous solutions by cellulose modified with D-glucose quaternary ammonium groups. Cellul. Chem. Technol. 46 (5-6), 319−329.

Zhou, X., Jing, G., Lv, B., Zhou, Z., Zhu, R., 2016. Highly efficient removal of chromium(VI) by Fe/Ni bimetallic nanoparticles in an ultrasound-assisted system. Chemosphere 160, 332−341.

Zhu, H., Kong, Q., Cao, X., He, H., Wang, J., He, Y., 2015. Adsorption of Cr(VI) from aqueous solution by chemically modified natural cellulose. Desalination Water Treat. 57 (43), 20368−20376.

https://doi.org/10.1016/j.heliyon.2019.e01491
2405-8440/© 2019 Published by Elsevier Ltd. This is an open access article under the CC BY-NC-ND license (http://creativecommons.org/licenses/by-nc-nd/4.0/).